EV2019
ELECTRIC VEHICLES INTERNATIONAL CONFERENCE & SHOW
www.evshow.ro
Icpe Solar Park
București, România
3-4 OCTOBER 2019

Electro-Thermo-Mechanical Behaviours of Laser Joints for Electric Vehicle Battery Interconnects

Usama F. Shaikh
WMG
The University of Warwick
Coventry, CV4 7AL, UK
Usama-Farooq-Shaikh.Shaikh@warwick.ac.uk

Abhishek Das
WMG
The University of Warwick
Coventry, CV4 7AL, UK
A.Das.1@warwick.ac.uk

Anup Barai
WMG
The University of Warwick
Coventry, CV4 7AL, UK
A.Barai@warwick.ac.uk

Iain Masters
WMG
The University of Warwick
Coventry, CV4 7AL, UK
I.G.Masters@warwick.ac.uk

***Abstract*— An automotive battery pack used in electric vehicle (EV) comprises several hundred to a few thousand of individual Lithium-ion (Li-ion) cells when cylindrical cells are used to build the battery pack. These cells are connected in series and/or parallel to deliver the required power and capacity to achieve the designed vehicle driving range. This triggers the need for suitable joining methods capable of providing mechanical strength together with the required electrical and thermal performances. A range of joining techniques are currently employed to connect large numbers of cells, and of these, laser welding is estimated to be the one of most efficient methods. Typically, the cylindrical cell casing is made of electrical grade steel which is electrically connected to copper tabs representing the cylindrical cell terminal to tab interconnect within the battery pack assembly. This study focuses on identifying the effect of laser welding process parameters on the mechanical, electrical and thermal responses of the laser welded joints produced using a 150 W Quasi-CW IR laser. Mechanical strength is assessed by evaluating the lap shear strength of the joint whereas the electrical and thermal responses are captured using voltage sensors and a thermal imaging camera respectively. It was observed that mechanical strength of the joint is highly correlated with electrical resistance and corresponding temperature raise at the joint. Furthermore, the optical micrographs reveal the microstructural characteristics of the joint.**

Keywords*— *EVs, laser welding, joint strength, weld microstructure, electrical resistance, temperature rise

I. INTRODUCTION

With increasing demand for electrification of automotive vehicles, development of durable and energy, efficient electrical drive systems is emerging as one of the key enablers for future e-mobility.

EVs, hybrid or plug-in hybrid vehicles (HEVs/PHEVs) consist of a battery pack which is composed of several modules each containing individual cells which are electrically and structurally joined to build the modules [1].

Applicability of joining methods to manufacture the modules, and subsequently, the battery packs is largely dependent on (i) type of cells to be used (i.e. cylindrical cell, pouch cell or prismatic cell) to build the battery pack, and (ii) critical-to-quality criteria such as mechanical strength, metallurgical compatibility, electrical resistance and thermal responses [2]. One of the main challenges associated with large number of electrical interconnects is to produce them with low joint resistance, low heat input and high mechanical strength to provide durability in harsh driving conditions [3]. Investigations are in progress on current and emerging joining methods to facilitate efficient joining.

For example, Das, et al. [2] have identified the suitable joining methods for cylindrical cell based battery pack building of which laser welding, micro-TIG welding and ultrasonic wedge bonding are the preferred joining methods. As dissimilar thin material joining is one of the key requirements for battery joining applications, several joining techniques are adopted to make satisfactory dissimilar interconnects, including ultrasonic metal welding [4], [5], ultrasonic wedge bonding [6], resistance spot welding [7], [8], soldering [9], micro-TIG welding [7], [10], micro-clinching [11] or laser welding [12]. Among these joining methods, laser welding provides several advantages over other joining methods including easy automation, contactless one-sided joining, high throughput, less heat input etc. However, proper fixturing is needed to ensure intimate contact between the mating parts for satisfactory joints [13], [14].

Additionally, Brand, et al. [13] had compared the electrical contact resistance obtained from resistance spot weld, ultrasonic weld and laser weld when CuZn37 tabs were welded on negative terminal of 26650 lithium-ion cells. Laser welding produced joints with the lowest contact resistance while satisfying the mechanical integrity. Therefore, laser welding has potential to be implemented as an efficient joining technique to replace current joining methods including resistance spot welding, micro-TIG welding or ultrasonic wire bonding for cylindrical cell based battery pack manufacture.

978-1-7281-0791-2/19/$31.00 ©2019 IEEE

However, detailed investigations are required to address the critical-to-quality criteria i.e. mechanical strength, electrical resistance and temperature rise (due to joule heating). Few research studies have been reported in the literature on joining dissimilar material focusing on individual quality criterion. To address the mechanical strength and microstructural behaviour, Hailat, et al. [15] conducted laser welding of two dissimilar materials, aluminium (Al) and copper (Cu), with and without tin foil alloy. Better lap shear strength and metallurgical compatibility were obtained due to the use of tin foil in between the Al and Cu. Similar to this, Schmalen, et al. [12] reported mechanical lap shear tests and metallographic analysis for laser welded Al-Cu connectors for Li-ion cells based battery assembly and formation of brittle intermetallic compounds.

Detailed mechanical and metallurgical characterisations were conducted by Solchenbach and Plapper [16] to identify robust parameter ranges and a maximum shear strength of 121 MPa was obtained from Al-Cu connection. Therefore, most of the studies are focused on the Al-Cu connections whereas in-depth investigations are not conducted on steel to Cu joints which is representative of the cylindrical cell to Cu lattice connection.

Apart from the mechanical and microstructural characterisation, two other important critical-to-quality criteria are electrical resistance and joule heating during the flow of electrical current. Limited research was conducted on contact resistance characterisation and subsequent temperature rise. Solchenbach, et al. [17] reported electrical contact resistance when laser welding was used to produce Al-Cu interconnects and they obtained the lowest contact resistance and highest mechanical interface strength with the same process parameters. Contact resistance from laser welding was lowest when compared with resistance spot welding, ultrasonic welding, and soldering [9], [13]. In addition, these contact resistances lead to Joules Heating which cannot be neglected as heat generation during battery charging and discharging may be significant for battery safety.

For example, Das, et al. [18] reported significant rise of temperature due to application of high current thought ultrasonic joints. In case of 0.3 mm Al tab to 1 mm Cu busbar ultrasonic joint, a temperature rise of 73.25 °C was reported when 250 amp current was applied for 60 sec whereas 49.02 °C was recorded for 0.3 mm nickel-plated copper (Cu[Ni]) tab to 1 mm Cu busbar joint. Furthermore, they extended their study to investigate the effect of tab-to-busbar joints under varying busbar thickness where electrical contact resistance and corresponding temperature rise were compared [19].

Excessive heating can cause premature ageing of the battery and beyond 70 °C can pose a safety risk as it exceeds the safe operating limits of the Li-ion cell [20], [21]. Therefore, detailed investigations are required to characterise the laser joints for evaluation of electrical resistance and corresponding temperature rise. To address the aforesaid challenges, this paper aims to identify the effects of laser processing parameters on:

- Mechanical strength and joint microstructure
- Change of joint resistance due to application of high current (amp)
- Rise in joint temperature due to the effect of joule heating.

The remainder of the paper is arranged as follows: section II describes the laser experimental details, set-ups for mechanical, electrical and thermal characterisations, section III analyses the results, and section IV draws the conclusions.

II. Materials and Experimental Details

A. Materials

In general, the Lithium-ion (Li-ion) cylindrical cell case is made of nickel-plated steel, such as Hilumin which is an electro nickel-plated diffusion annealed steel strip for battery applications where low contact resistance and high corrosion resistance are needed [22]. Nickel-plated copper strips are commonly used as tabs to connect the cylindrical cells to the busbar. These two materials each 0.3 mm thick were used in this experimental investigation and their corresponding chemical composition are given in Table I.

TABLE I. Material Details

Material	Specification	Chemical Composition (wt. %)
Steel-Hilumin	DC04 LC; EN 10139/10140	C= 0.047, Mn=0.235, P=0.011, S=0.010 Al=0.059, Si=0.002, Bo=0.0019 Fe-balance
Copper (Cu)	C101S; BS 2870	O=0.008, Pb=0.001, Bi=0.005, Cu-balance

B. Laser welding set-up

Pulsed laser welding was carried out using an IPG 150W Quasi-CW IR laser optical head in which a wobble head was integrated. The wobble head was capable of producing wobble in various motions such as circular counter clockwise (CCW), circular clockwise (CW), infinity and figure of 8. For this investigation, CW motion was used and laser welding process parameters with their corresponding ranges are given in Table II. In the initial screening study, the parameter ranges were identified based on machine specification and welding requirement.

TABLE II. Welding Parameters and Ranges

Category	Parameter	Range
Wobble parameter	Frequency	1-1000 Hz
	Amplitude	0.1-0.9 mm
Laser parameter	Power	1-100% (1.5 kW peak power)
	Frequency	1-100 Hz
	Pulse on time	1-10 msec
Machine parameter	Speed	1-1500 mm/min
	Focus range	±1.0 mm

Figure 1 shows the schematic of test sample where 15 mm long linear stitch was places at the centre of the overlap region. Additionally, to ensure intimate contact between Cu and Hilumin sheets, a customised fixture was developed to hold both the sheets together during welding. Figure 2(a) shows the fixture with two quick release clamps which keeps the sheets in place and removes the part-to-part gap.

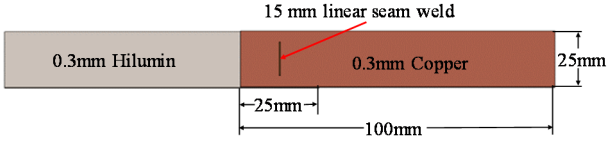

Fig. 1. Schematic of test sample with laser weld.

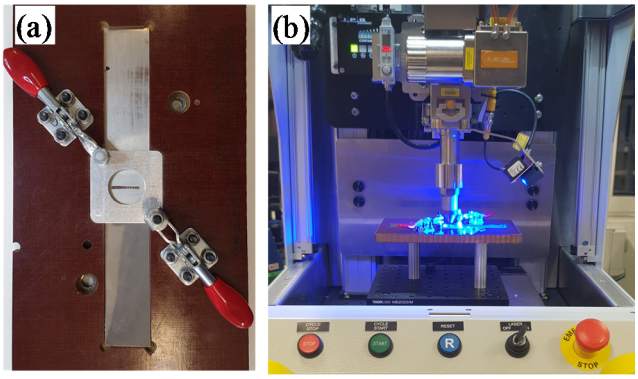

Fig. 2. Laser welding (a) fixture to ensure intemate contact, and (b) set-up.

The laser welding set-up with the fixture is shown in Figure 2(b). The effects of parameter changes were identified in two stages. Firstly, based on the joint strength obtained in the pilot stage, the wobble amplitude, wobble frequency and focus position were identified and kept then at 0.4 mm, 400 Hz and on top surface respectively. Thereafter, process parameters such as laser power, pulse on time, pulse frequency and welding speed (at 30% and 40% of peak power, i.e. P30% and P40%) were chosen to characterise the mechanical, electrical and thermal behaviours (see Table III).

TABLE III. COMBINATION OF PROCESS PARAMETERS

Sr. No.	*Id*	*Level*	*Power [%]*	*Speed [mm/min]*	*Pulse on Time [mS]*	*Frequency [Hz]*
Power Modulation						
1	A1	L1	30	1500	2	50
2	A2	L2	40	1500	2	50
3	A3	L3	50	1500	2	50
Pulse on Time Modulation						
4	A4	L1	40	1500	1	50
5	A2	L2	40	1500	2	50
6	A5	L3	40	1500	3	50
Frequency Modulation						
7	A6	L1	40	1500	2	30
8	A2	L2	40	1500	2	50
9	A7	L3	40	1500	2	70
Speed Modulation at P40%						
10	A8	L1	40	500	2	50
11	A9	L2	40	1000	2	50
12	A2	L3	40	1500	2	50
Speed Modulation at P30%						
13	A10	L1	30	500	2	50
14	A11	L2	30	1000	2	50
15	A1	L3	30	1500	2	50

C. *Set-up for mechanical testing*

The weld quality of a joint was evaluated by the maximum load it could withstand during mechanical testing. Lap shear tests were carried out on weld specimens to understand the effect of the process parameters. The lap shear test specimen was gripped using wedge grips on an Instron 3367 static test frame with 30 kN calibrated load cell. Tests were carried out at a speed of 2 mm/min. The grip set-up with the test specimen is shown in Figure 3(a).

Maximum load was recorded for each test. For each test combination, the average of three repeats were calculated. Depending on the load-displacement characteristic of weld specimen and cross-sectional micrographs, welds were classified into three categories, under-weld, over-weld and good-weld. Details of this classification are discussed in results and discussions – joint microstructure section.

D. *Set-up for electrical and thermal analysis*

To investigate changes in electrical resistance and relative rise in temperature of joints, lap configuration samples were produced using the parameter combinations from TABLE III. Table III. The test set-up was designed to carry out both tests simultaneously as shown in Figure 3(b). Test set-up consists of two brass blocks, 165 mm apart mounted on an acrylic base. The joint specimen is mounted between brass block and 75 amp current is made to flow through the specimen for 120 seconds. Keeping the weld seam at the center, voltage drop points were marked at 25 mm on both side (i.e. 50 mm apart) and another two 25 mm apart voltage drop points were fixed on both the parent materials. Therefore, the voltage drop was measured along the length of specimen at six different marked points. Along with voltage drop, thermal camera FLIR T440 was used to capture rise in joint temperature. To improve efficiency of thermal camera, silicon spray was used to reduce reflection on the test specimen.

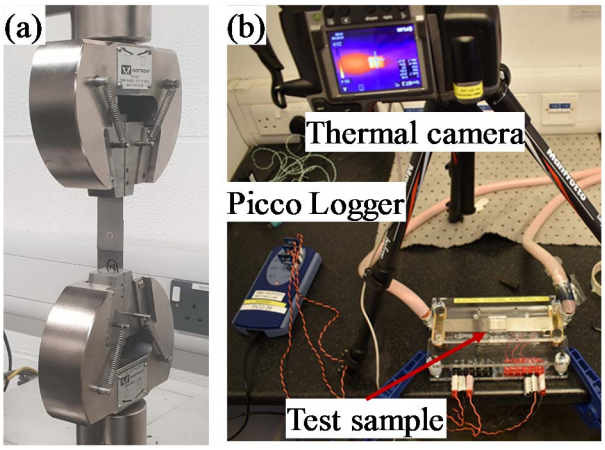

Fig. 3. Set-up for (a) mechanical, and (b) electrical & thermal tests.

III. RESULT AND DISCUSSION

The effects of process parameters under investigation were evaluated based on mechanical lap shear strength, joint microstructure, electrical resistance and temperature rise.

A. *Joint strength behaviour*

Joint strength of weld was evaluated by performing the lap shear test with three repeats for each combination from Table III. The effect of process parameters on the lap shear load is given in Figure 4. There is steep increase in maximum load from level one to two of power modulation (i.e. 30% to 40%), pulse on time modulation (i.e. 1 to 2 milliseconds) and frequency modulation (i.e. 30 to 50 Hz). This is due to the fact that at higher power, pulse on time and frequency make the joint stronger by moving it from under-weld (i.e. intermittent contact or insufficient penetration depth) to good-weld (good penetration and interface width). However, maximum load remained almost at same level from level two to three for power modulation and pulse on time modulation whereas for frequency modulation load shows linear trend from 788N to 988N.

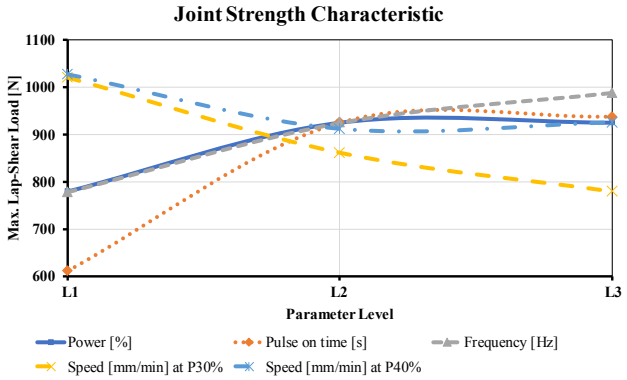

Fig. 4. Effect of process parameters on lap shear load.

Maximum load of 1027 N was achieved at the low speed of 500 mm/min with power level 40%. As the speed increases, maximum joint load decreases in almost linear pattern for speed modulation when power at 30%. Joint behaviour indicates that, load characteristic depends on weld geometrical microstructure (i.e. interface width or penetration depth) due to mixing of both the materials during welding which is shown in next section.

B. Joint microstructure

Joint microstructure was evaluated using the optical microscope during the investigation. Interface width represents the cross-sectional length of weld interface of both the materials and penetration depth represents the depth of weld pool from the interface into the lower material. In this study, under-weld was considered when the penetration depth was less than 0.3 times of thinnest material thickness and over-weld when more than 0.8 times of lower material or full penetration was obtained. In between, good-weld was obtained. Figure 5 shows the representative joint microstructures obtained from various parameter combinations. For example, power level modulation A1 have least penetration of 53 µm as shown in Figure 5 (A1).

The effects of process parameters on the penetration depth and interface width are shown in Figure 6 and Figure 7 respectively. As per the microstructure characteristics, power and speed had a high influence on penetration depth. With increase in power, penetration depth was increased as higher energy created a larger weld pool, whereas increasing speed had lower penetration depth due to shallow melt pool.

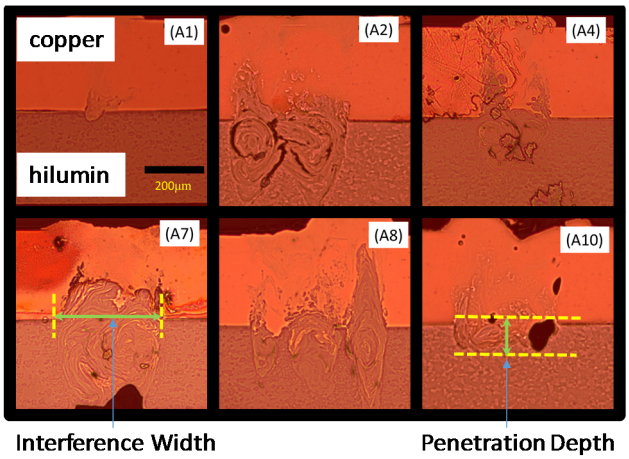

Fig. 5. Joint microstructure images showing the penetration depth and interface width for few parameter combinations listed in Table III.

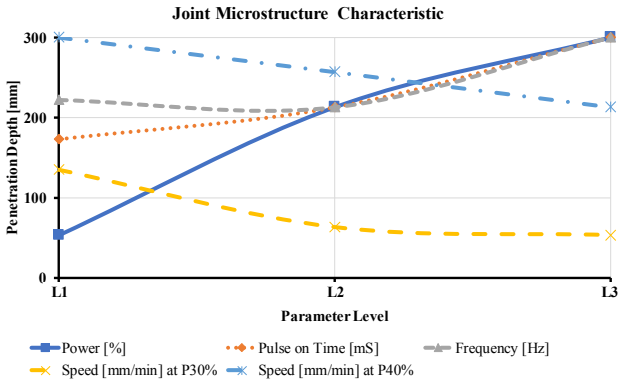

Fig. 6. Effect of process parameters on the penetration depth.

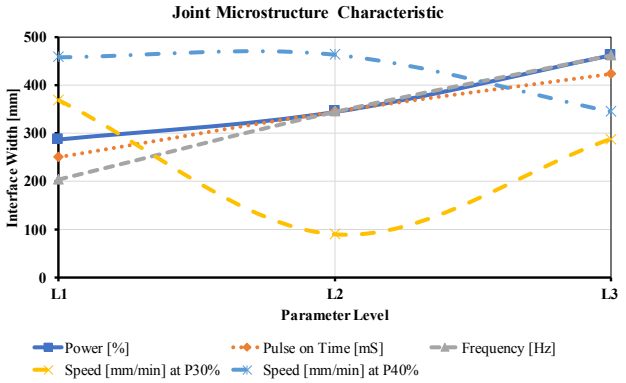

Fig. 7. Effect of process parameters on the interface width.

Similarly, interface width was more dependent on power, frequency and pulse on time, as a larger melt pool created a bigger interface width. Interface width was maximum of 462 µm for combination A8 as shown in Figure 5 (A8).

C. Joint resistance

An equivalent joint resistance circuit helps in understanding the joint resistance behavior as number of resistances were present. Joint resistance was calculated based on the corresponding voltage drop as shown in Figure 8. The resistance of the joint with overlap (i.e. $R_{J\&O}$ which varies with different combination of parameters) is compared with parent metal resistance (i.e. R_{Hi} and R_{Cu} for Hilumin and copper, respectively) using resistance K factor [23]. For dissimilar metal joints, K factor can be calculated as per (1):

$$K = \frac{R_{J\&O}}{R_{Hi}+R_{Cu}} \quad (1)$$

If K equals to 1, $R_{J\&O} = R_{Hi} + R_{Cu}$, which indicates no joint resistance is observed as overlap region is same as parent metal resistance.

The K-factor based resistance behaviour graph is shown in Figure 9. Joint resistance characteristic graphs shows slight changes in resistance factor throughout all the combinations. Resistance is least for frequency modulation at 50 Hz frequency which indicated less intermixing of dissimilar materials.

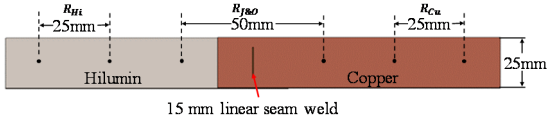

Fig. 8. Schematic of joint resistance measurement set-up.

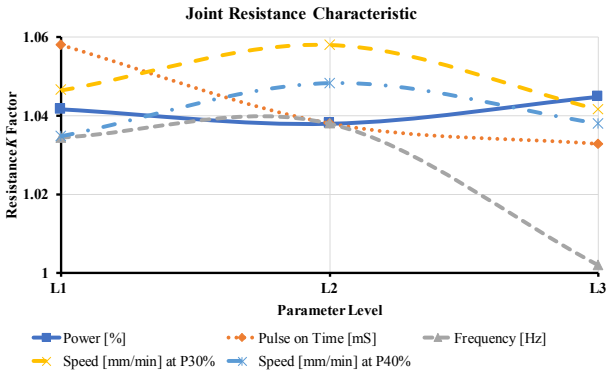

Fig. 9. Effect of process parameters on the *K*-factor.

For other combination, resistance *K* factor lies in between 1.03 to 1.06. Pulse-on time modulation shows almost linear decrease in resistance with increase in pulse-on time. Furthermore, a similar decreasing trend was observed for frequency which can be attributed to more surface contact obtained due to higher frequency and pulse-on time. Maximum joint resistance peaks for both speed modulation. Both the speed modulations at P30% and P40% showed similar trend on joint resistance behaviour. However, the change in resistance for all combinations are relatively small compared to parent material.

D. Joint temperature characterisation

Maximum joint temperature characterisation graph helps investigation of the rise of joint temperature when current is passed through the joint due to the effect of joule heating. The range of change in temperature was between 72.47 °C to 78.49 °C for 75 amp current passed for 120 sec (see Figure 10). It was also observed that joint temperature decreased with increase in pulse-on-time, frequency and speed at power 30%. But in event of power 40% speed modulation, temperature decreases from speed 500 mm/min to 1000mm/min and again it increases with the speed. The maximum change of temperature is 6.35% for power 30% speed modulation followed by 5.06% for frequency modulation. For other modulation, the change of temperature is within 3-4 °C.

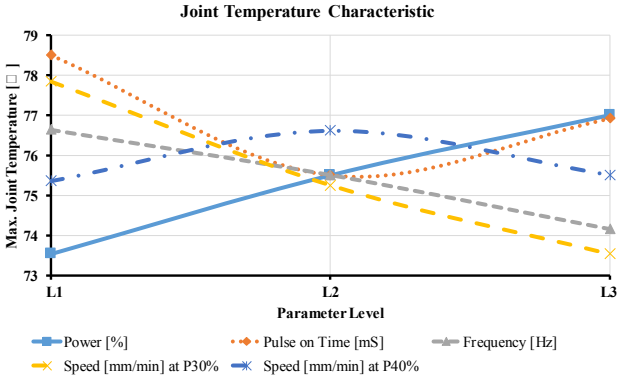

Fig. 10. Effect of process parameters on the temperature rise at the joint.

E. Correlation between joint strength and resistance

The maximum joint strength obtained from all the process parameter combinations (i.e. A1 to A11) were arranged from minimum to maximum values and corresponding joint resistance values were plotted on the same graph (see Figure 11) for the investigation of correlation between both.

Logarithmic trend lines were used to understand the change in behaviour between joint strength and resistance.

According to Figure 11, it can be observed that both the maximum joint strength and maximum joint resistance follow the same trend. It can be conclude that to obtain higher strength more mixing of steel and copper was achieved and this resulted in slightly higher resistance.

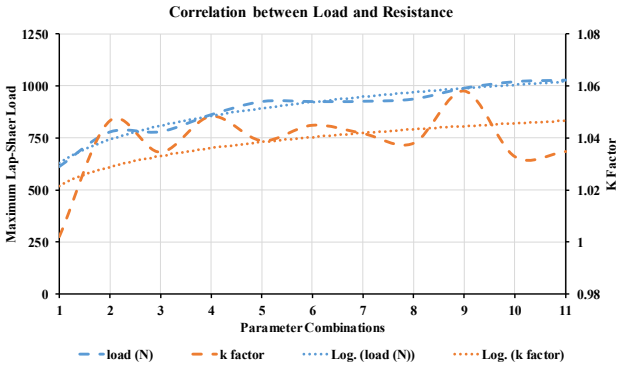

Fig. 11. Correlation between lap shear load and joint resistance

IV. Conclusions

This study characterised the effects of pulsed laser process parameters (i.e. laser power, pulse on time, pulse frequency and welding speed) on mechanical lap shear strength, weld geometrical characteristics, electrical resistance and temperature rise at the joint. Nickel-coated copper (Cu[Ni]) was laser welded with nickel-coated steel (i.e. electrical grade Hilumin) which is representative of commercial cylindrical cell to copper tab interconnects used in EV batteries. Using this dissimilar material combination, the effects of process parameters on electro-thermo-mechanical behaviours of laser joints were identified.

This paper significantly explores the following areas:

- Laser power, pulse on time and frequency had positive correlation with the lap shear strength while speed had exhibited negative correlation. A maximum lap shear load of 1.02 kN was obtained when the laser power was at 40%, speed at 500 mm/min, pulse on time at 2 ms and frequency at 50 Hz.
- Joint geometrical characteristics (i.e. interface width and penetration depth) were used to identify the under-weld, good weld and over-weld. A maximum interface width of 462 µm was obtained with the combination of process parameters in A8. Laser power had most influential effect on penetration depth as under-weld, good-weld and over-weld were obtained at three power levels.
- Electrical resistance of the joint with overlap is compared with parent metal resistance using resistance *K* factor. Joint resistance characteristic showed slight changes in resistance factor throughout all the combinations which were relatively small compared to change in resistance in parent materials.
- Due to effect of joule heating, rise in joint temperature was obtained when current was passed through the joint. The range of change in temperature was between 72.19 °C to 78.49 °C for 75 amp current passed for 120 sec.

Similar to resistance behavior, the change in temperature for all combinations are relatively small and the main temperature increase was due to parent material.

- Positive correlation between joint strength and corresponding electrical resistance was obtained. To obtain higher strength more mixing of steel and copper was occurred and this may resulted in slightly higher resistance.

This study established the genetic electro-thermo-mechanical behaviours of pulsed laser welded joints. Furthermore, detailed analysis is required to understand the formation of intermetallic and its effect on critical-to-quality criteria. Therefore, future investigations will explore the in-depth analysis of joint microstructure in relation with electrical resistance and temperature rise.

ACKNOWLEDGMENT

This research has been partially supported by WMG Centre High Value Manufacturing (HVM) Catapult at The University of Warwick and Jaguar Land Rover Limited, UK.

REFERENCES

[1] A. Väyrynen and J. Salminen, "Lithium ion battery production," The Journal of Chemical Thermodynamics, vol. 46, pp. 80-85, 2012.

[2] A. Das, D. Li, D. Williams, and D. Greenwood, "Joining Technologies for Automotive Battery Systems Manufacturing," World Electric Vehicle Journal, vol. 9, no. 2, pp. 22, 2018.

[3] S. S. Lee, T. H. Kim, S. J. Hu, W. W. Cai, and J. A. Abell, "Joining Technologies for Automotive Lithium-Ion Battery Manufacturing: A Review," ASME International Manufacturing Science and Engineering Conference, Pennsylvania, USA, 2010, vol. 1, pp. 541-549.

[4] M. Shakil, N. H. Tariq, M. Ahmad, M. A. Choudhary, J. I. Akhter, and S. S. Babu, "Effect of ultrasonic welding parameters on microstructure and mechanical properties of dissimilar joints," Materials & Design, vol. 55, pp. 263-273, 2014.

[5] A. Das, I. Masters, and D. Williams, "Process robustness and strength analysis of multi-layered dissimilar joints using ultrasonic metal welding," Int J Adv Manuf Technol, vol. 101, no. 1, pp. 881-900, 2019.

[6] H. Ji, M. Li, C. Wang, J. Guan, and H. S. Bang, "Evolution of the bond interface during ultrasonic Al–Si wire wedge bonding process," Journal of Materials Processing Technology, vol. 182, no. 1, pp. 202-206.

[7] A. Das, D. Li, D. Williams, and D. Greenwood, "Weldability and shear strength feasibility study for automotive electric vehicle battery tab interconnects," Journal of the Brazilian Society of Mechanical Sciences and Engineering, vol. 41, no. 1, p. 54, 2019.

[8] Y. Zhou, P. Gorman, W. Tan, and K. J. Ely, "Weldability of thin sheet metals during small-scale resistance spot welding using an alternating-current power supply," Journal of Electronic Materials, vol. 29, no. 9, pp. 1090-1099.

[9] M. J. Brand, E. I. Kolp, P. Berg, T. Bach, P. Schmidt, and A. Jossen, "Electrical resistances of soldered battery cell connections," Journal of Energy Storage, vol. 12, pp. 45-54, 2017.

[10] (2017-07-06). Micro TIG Welding [Online]. Available: http://www.amadamiyachi.com/products/micro-tig.

[11] J. Varis, "Ensuring the integrity in clinching process," Journal of Materials Processing Technology, vol. 174, no. 1, pp. 277-285, 2006.

[12] P. Schmalen, P. Plapper, and W. Cai, "Process Robustness of Laser Braze-Welded Al/Cu Connectors," SAE Int. J. Alt. Power., vol. 5, no. 1, pp. 195-204, 2016.

[13] M. J. Brand, P. A. Schmidt, M. F. Zaeh, and A. Jossen, "Welding techniques for battery cells and resulting electrical contact resistances," Journal of Energy Storage, vol. 1, pp. 7-14, 2015.

[14] A. Das, P. Franciosa, and D. Ceglarek, "Fixture design optimisation considering production batch of compliant non-ideal sheet metal parts," Procedia Manufacturing, vol. 1, pp. 157-168, 2015.

[15] M. M. Hailat, A. Mian, Z. A. Chaudhury, G. Newaz, R. Patwa, and H. J. Herfurth, "Laser micro-welding of aluminum and copper with and without tin foil alloy," Microsystem Technologies, vol. 18, no. 1, pp. 103-112, 2012.

[16] T. Solchenbach and P. Plapper, "Mechanical characteristics of laser braze-welded aluminium–copper connections," Optics & Laser Technology, vol. 54, pp. 249-256, 2013.

[17] T. Solchenbach, P. Plapper, and W. Cai, "Electrical performance of laser braze-welded aluminum–copper interconnects," Journal of Manufacturing Processes, vol. 16, no. 2, pp. 183-189, 2014.

[18] A. Das, T. R. Ashwin, and A. Barai, "Modelling and characterisation of ultrasonic joints for Li-ion batteries to evaluate the impact on electrical resistance and temperature raise," Journal of Energy Storage, vol. 22, pp. 239-248, 2019.

[19] A. Das, A. Barai, I. Masters, and D. Williams, "Comparison of tab-to-busbar ultrasonic joints for electric vehicle Li-ion battery applications," presented at the Electric Vehicle Symposium, Lyon, France, 2019.

[20] F. Leng, C. M. Tan, and M. Pecht, "Effect of Temperature on the Aging rate of Li Ion Battery Operating above Room Temperature," Scientific reports, vol. 5, pp. 12967-12967, 2015.

[21] T. M. Bandhauer, S. Garimella, and T. F. Fuller, "A Critical Review of Thermal Issues in Lithium-Ion Batteries," vol. 158, no. 3, pp. R1-R25, 2011.

[22] https://www.tatasteeleurope.com/en/products/engineering/electro-plated/hilumin. (23-05-2019)

[23] V. Dimatteo, A. Ascari, and A. Fortunato, "Continuous laser welding with spatial beam oscillation of dissimilar thin sheet materials (Al-Cu and Cu-Al): Process optimization and characterization," Journal of Manufacturing Processes, vol. 44, pp. 158-165, 2019.